ACADEMIA ROMÂNĂ
*Revue Roumaine de Chimie*
http://web.icf.ro/rrch/

*Rev. Roum. Chim.,*
**2018**, *63*(4), 337-346

# THE SYNTHESIS, CHARACTERISATION AND CATALYTIC PERFORMANCE OF PLATINUM ENCAPSULATED MESOPOROUS SODALITE MATERIAL

Da XUE,[a,b] Fan LIU,[a] Huan GAO,[a] Lu YANG,[a] Yibo WU,[a] Weijian XUE,[a] Zhiping LV[a] and Fuxiang LI*[a]

[a] College of Chemistry and Chemical Engineering, Taiyuan University of Technology, People's Republic of China
[b] Shanxi Coking Coal Group Co.,Ltd People's Republic of China

*Received December 12, 2017*

Pt nanocluster encapsulated sodalite (PtSOD) with mesoporous structure was successfully synthesized through cation exchange and Pt $(NH_3)_4Cl_2$ as precursor of Pt by direct hydrothermal synthesized (PtSOD-M). The obtained products were characterized by XRD, $N_2$ adsorption-desorption, temperature programmed desorption (TPD, $H_2$), SEM and TEM. The sample PtSOD-Ni$(CH_3COO)_2$ showed the high surface area (114.6 $m^2/g$) and the PtSOD-Zn $(NO_3)_2$ showed the large pore volume (0.44 $cm^3/g$). The catalytic activities of PtSOD-M were evaluated with benzene hydrogenation reactions. The PtSOD-Ni$(CH_3COO)_2$ catalyst during hydroprocessing of benzene with 91.5% conversion for cyclohexane showed improved catalytic activity compared to the Na-form sodalite with solely microporous structure.

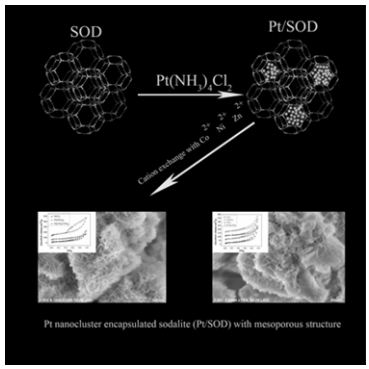


## INTRODUCTION

Zeolites are uniform microporous crystalline materials composed by a regular array of aluminosilicate minerals in the molecular dimension.[1-3] Zeolites have outstanding properties such as excellent activity, stability, molecular size-selective and shape-selective. Results of these properties, zeolites are widespread used in the industry for catalysis, adsorption, separation and ion-exchange processes.[4-8] Noble metals are highly active, selective and stable in many important industry reactions like hydrogenation, aromatization, hydrodearomatization etc., and these metals are finely dispersed as nanoclusters on porous supports mostly used in supported form to maximize the active surface area. The catalytic properties are drastically changed with the size of the metal clusters which it further decreases to a sub-nanometre scale or ultimately to an atomic level.[9-19] Mainly difficulties of the metal nanoclusters disperse in porous supports which in dispersion control, low stability against sintering and poisoning by certain reactions.[20-24] The mineral sodalite was first described in 1811 by Thompson and its structure was solved in 1930 by Pauling with the chemical composition $Na_8[AlSiO4]_6Cl_2$. The framework of sodalite completely consists of sodalite cages (regular truncated octahedral cages). These cages are composed of six four-member rings and eight six-member rings. Therefore, it is the smallest pore size among all zeolites about 2.8 Å.[25, 26] Sodalite have been very little studies on the catalytic application due to the low surface area and the limitation of pore structure. Nanoclusters of metals are dispersed in sodalite cages and the cages protect the metals, selectively provide access to some molecules (with kinetic diameter <2.8 Å

* Corresponding author: Prof. Fuxiang Li; Fax: +86 0351 6111178 Phone: +86 0351 6010550 E-mail address: L63f64x@163.com

like $H_2$) but block the poisons (with kinetic diameters of >2.8 Å such as sulfur compounds) and coke precursors from reaching the active metal sites.[27-29] Sibi[29] reported a catalyst with Pt incorporated inside sodalite cages encapsulated in ZSM-5 supported with Ni and Mo and as a hydrocracking catalyst for the conversion of triglycerides to kerosene and diesel. Such sintering and poisoning can be avoided by designing catalysts where metal clusters in the sodalite cages that only small $H_2$ can access but larger organic reactants cannot. So they need sodalite cages encapsulated in ZSM-5. Since the metal clusters are encapsulated in cages of sodalite so organic molecules cannot directly contact or diffuse to the metal clusters. The catalytic activities could be attributed to the hydrogen spillover at the external surface of ZSM-5 which acted as hydrogen spillover acceptor. In principle, mesoporous or nanocrystalline sodalite with stronger basicity and higher surface areas could be used as a kind of basic solid catalyst supporter and exhibited catalytic activities.[30-35] Development of mesoporous structures has been reported using hard[36-39] and soft[1, 40-45] templating techniques during the hydrothermal route or post-treatment procedure. Nevertheless, as compared with conventional zeolite, such modified mesoporous materials also carry serious limitations and drawbacks due to weak basicity and low hydrothermal stability which limits their use as catalysts in a wide range of industrial processes. However, the use of ion exchange resin has not been reported for the formation of ordered mesoporous sodalite materials. [46-48]

As mentioned above, this work reports the synthesis of the encapsulation of Pt nanoclusters within sodalite cage (PtSOD) and modified by ion exchange with $Co^{2+}$, $Ni^{2+}$ and $Zn^{2+}$(PtSOD-M). PtSOD-M with a higher surface area and a larger pore volume attributed to the presence of mesoporous structures. We investigated and characterized the sample catalytic activity by hydrogenation of benzene. Also we compared catalytic performance of PtSOD-M series and Na-form PtSOD.

## EXPERIMENTAL

### 1. Synthesis of catalysts

All the chemicals, including sodium aluminate ($NaAlO_2$, Tianjin Kermel Chem. Reagent Co.Ltd.), sodium metasilicate ($Na_2SiO_3 \cdot 9H_2O$, Tianjin Kermel Chem. Reagent Co. Ltd.), $Pt(NH_3)_4Cl_2$ (Xi'An Catalyst Chem. Co. Ltd. ), distilled $H_2O$, were used as received without further purification. The homogeneous synthesis gel has a molar composition of $m[Pt(NH_3)_4Cl_2]$:m[Si-Al gel]=0.0636 : 0.032. It was crystallized at 373K for 12 h in a 100 mL Teflonlined stainless steel autoclave. The product (designated as PtSOD) was filtered thoroughly, washed with distilled water, dried at 393K for 2 h and calcined at 773K for 4 h.

### 2. Cation exchange of catalysts

Cation exchange of Na-form PtSOD of all the catalyst samples was performed with 0.1 M solutions of $Co^{2+}$, $Ni^{2+}$ or $Zn^{2+}$. One gram of the Na-form PtSOD was stirred with 5 mL of the solution at 293 K for 2 h. This procedure was performed three times in all to ensure maximum cation exchange. The resultant mixture was filtered and washed repeatedly with distilled water until it was free from physisorption metal ions. The resulting exchanged materials were dried at 373 K for 12 h. They were subsequently calcined in air at 773 K for 5 h. *i.e.*, $CoCl_2$ exchanged PtSOD (PtSOD-$CoCl_2$).

### 3. Catalyst characterization

XRD pattern was recorded on a Shimadzu X-ray diffractometer LabX XRD-6000 with CuKα radiation. The related parameters were set as follows: a wave length of 0.15418 nm, a step length of 0.02°, a scanning rate of 8 deg/min, a voltage of 40 kV, and a current of 30 mA.

The pore textural properties of different spillover hydrogen receptors were determined by nitrogen adsorption-desorption measurements at 77 K using a Quantachrome NOVA 2000e. The samples were outgassed in vacuum at 673 K for 3 h prior to measurements. The total surface area was calculated based on the BET method in the relative pressure range of 0.05 ~ 0.4. The mesopore volume was analyzed by the t-plot method at $P/P_0$=0.99.

Temperature programmed desorption of hydrogen ($H_2$-TPD) was carried out on a chemisorption analyzer FINESORB-3010. The mixture samples consisted of 15 mg of PtSOD catalyst and 15 mg of spillover hydrogen receptor (50 wt %). They were pretreated at 450 °C for 2 h and cooled in flowing argon. The carrier gas and adsorbed gas were Ar and a gas mixture of $H_2$ and $Ar_2$ (10 vol% $H_2$ in argon), respectively. The adsorption time was 40 min in ambient temperature. $H_2$-TPD profiles were obtained at the temperature and current of TCD thermal conductivity cell controlled in 60 °C and 80 mA, respectively. The desorption temperature was ramped at 20 °C / min.

Transmission electron micrograph (TEM) images were obtained with a Tecnai G2F30 microscope at an operating voltage of 300 kV. Scanning electron microscopy (SEM) was conducted using a Hitachi S-4800 microscope operating at 2 kV without a metal coating.

### 4. Catalytic activity measurements

Hydrogenation of benzene (1% benzene in undecane) was carried out in a 50 mL stainless steel autoclave. The pretreated samples (0.2 g of catalysts (Na-form PtSOD with spillover hydrogen receptors in 1:1 mass ratio or 0.2g PtSOD-M) and 2 mL benzene solution were added into the autoclave. The sealed reactor was pressurized with hydrogen to 3 MPa at 373 K. The reaction was maintained for 3 h at a stirring speed of 500 rpm.

The reactants and products were analyzed by a gas chromatograph with a flame ionization detector (FID). The capillary column the type of which was PEG-20M 30m*0.25mm*0.5μm was used and its temperature was controlled at 353 K. The temperatures of the vaporizing chamber and testing room were both 473 K.

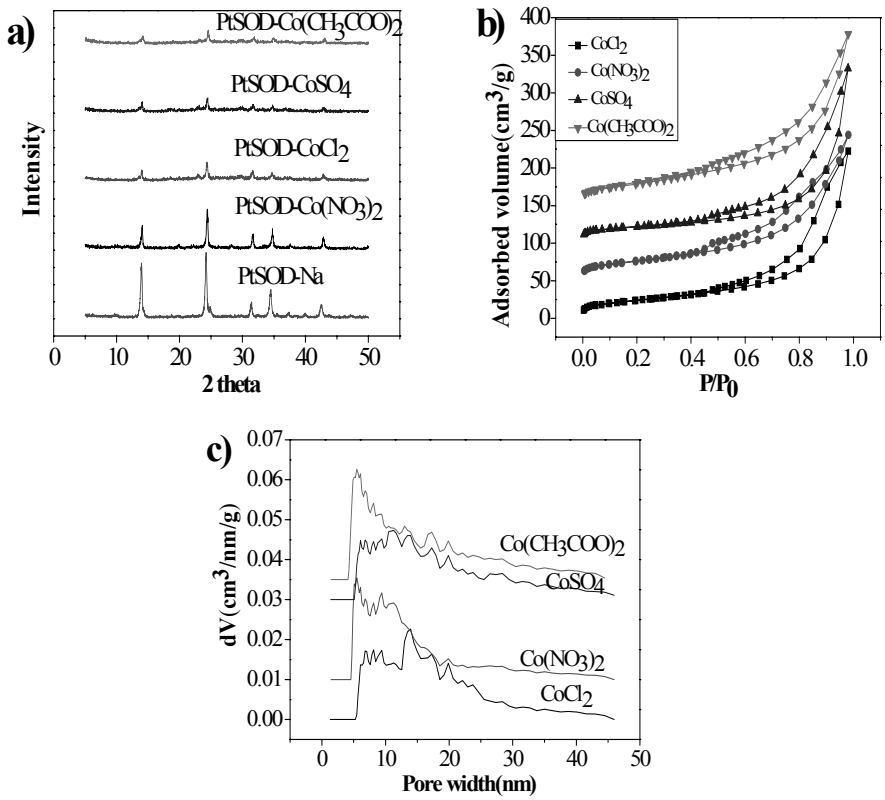


Fig. 1 – PtSOD exchange with $Co^{2+}$; a) XRD patterns; b) $N_2$ adsorption-desorption isotherms; c) DFT pore size distribution.

## RESULTS AND DISCUSSION

Wide angle XRD patterns of PtSOD and PtSOD-Co series consisted of peaks that were typical of sodalite (Fig.1.a)). The two prominent peaks at 2theta =13.9°and 24.3°represented (110) and (211) crystal planes, respectively.[26] Although the peak of PtSOD-Co$(C_2H_5O)_2$, PtSOD-$CoSO_4$, PtSOD-$CoCl_2$, PtSOD-Co$(NO_3)_2$ intensity decreases it was also suggested that the sodalite structure was retained after ion exchange and calcination steps. Fig. 1.b) shows a $N_2$ adsorption–desorption isotherm of representative type IIb curve with abrupt change in the relative pressure range of 0.8–0.9, where the mesoporosity only arises from interparticle interactions. The type H3 hysteresis loops did not exhibit limiting adsorption at high $P/P_0$ and at $P/P_0$ of 0.5–1.0 and the two branches are nearly horizontal and parallel over a wide range, indicating the presence of aggregates of plate-like particles that gave rise to narrow slit shaped. As depicted in Table 1 the Brunauer–Emmet–Teller (BET) report that in the PtSOD-$Co^{2+}$ series the PtSOD-Co$(CH_3COO)_2$ has the highest surface area of 97.9 $m^2/g$ and the single point pore volume is 0.30 $cm^3g^{-1}$. A peak in the pore distribution at 6.1 nm is observed in Fig. 1.c) and Table 1, indicating relatively uniform mesopores. The rest PtSOD-Co series have similar mesoporous structures but the pore distribution is more extensive.

Fig 2.a) shows the XRD patterns of the PtSOD and PtSOD-Ni series consisted of peaks that were typical of sodalite except for PtSOD-Ni$(CH_3COO)_2$ when the peak at 2Theta= =13.9°and 24.3° almost disappeared. However the peaks of PtSOD-Ni$(NO_3)_2$, PtSOD-$NiCl_2$ maintain well. The samples PtSOD-Ni$(CH_3COO)_2$ and PtSOD-$NiCl_2$ had Type H3 loops and did not show limiting adsorption at high $P/P_0$. This is ascribed to the presence of aggregates of plate-like particles that gave rise to slit-shaped pores. The PtSOD-Ni$(NO_3)_2$ samples possessed Type H4 hysteresis loops, over a wide range of P/P0 values the two branches remained nearly horizontal and parallel, indicating the presence of narrow slit-like pores. The $N_2$ adsorption–desorption isotherm of PtSOD-Ni$(NO_3)_2$ and PtSOD-$NiCl_2$ are representative type IIb curve, type H3 hysteresis loop and are similar with PtSOD-Co series [Fig. 2.b)]. As described in Table 1 the Brunauer–Emmet–Teller (BET) report that, in the PtSOD-$Co^{2+}$ series, the PtSOD-Ni$(CH_3COO)_2$ has the highest surface area of 114.6 $m^2/g$ and the single point pore volume is 0.26 $cm^3g^{-1}$. The sample PtSOD-Ni$(CH_3COO)_2$ pore distribution at ~5 nm and concentrated is observed in Fig.2.c) and Table 1. PtSOD-Ni$(NO_3)_2$ and PtSOD-$NiCl_2$ pore distribution is much broader.

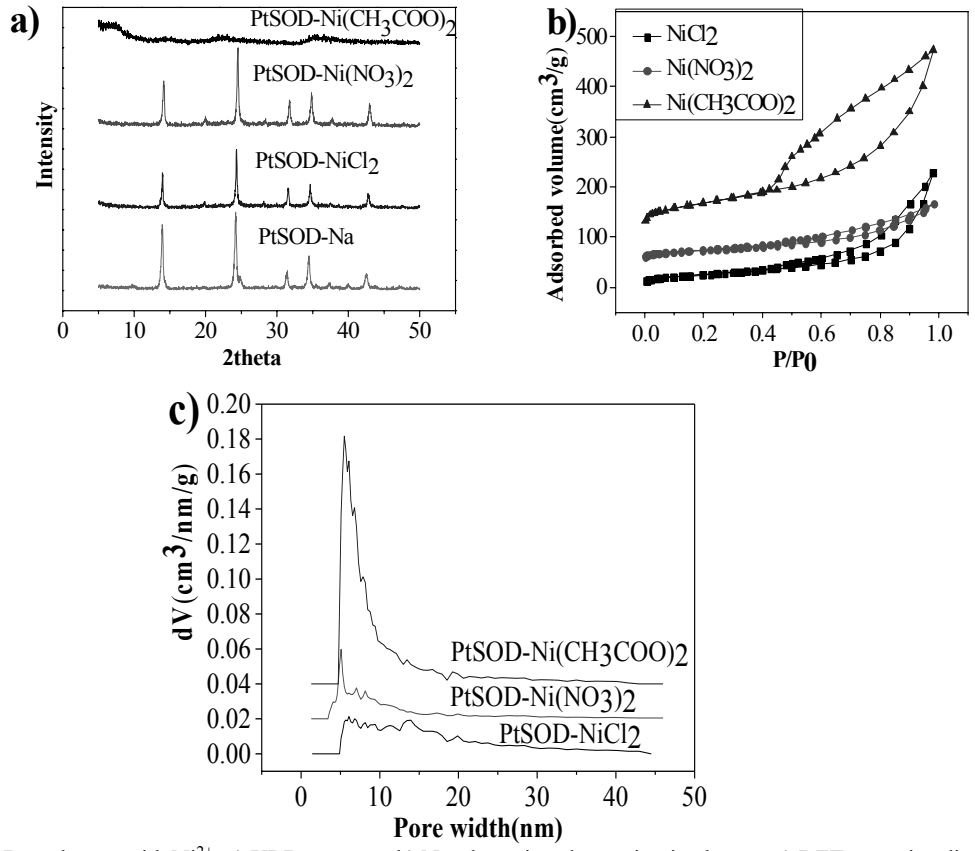


Fig. 2 – PtSOD exchange with $Ni^{2+}$; a) XRD patterns; b) $N_2$ adsorption-desorption isotherms; c) DFT pore size distribution.

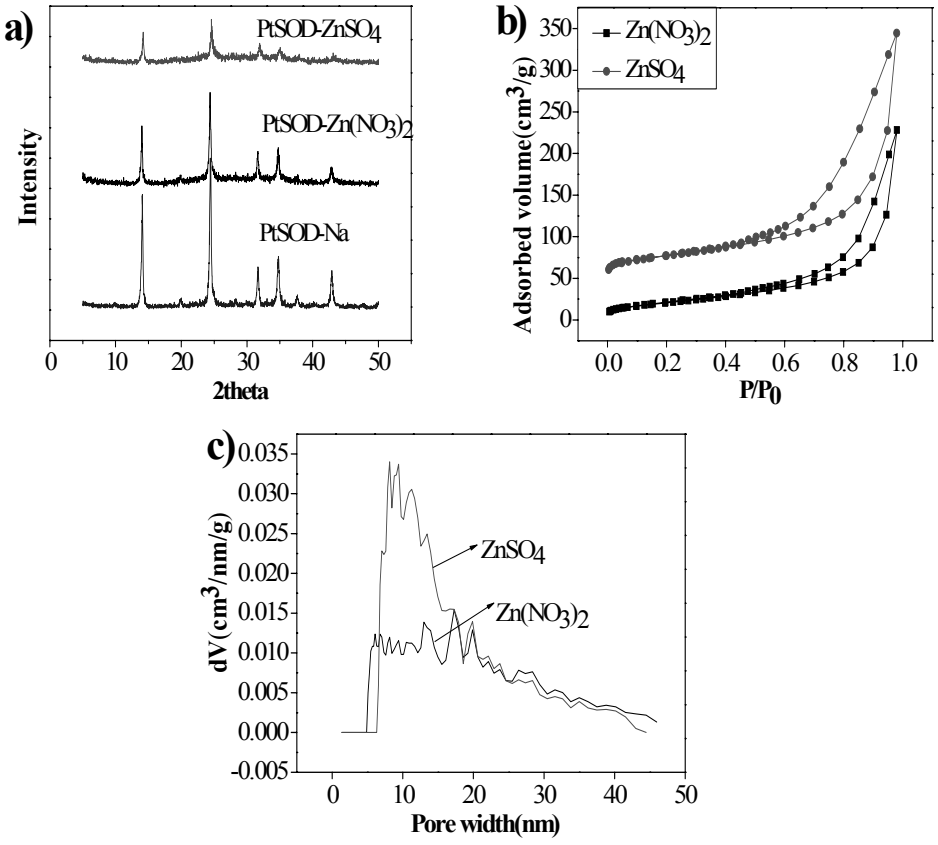


Fig. 3 – PtSOD exchange with $Zn^{2+}$; a) XRD patterns; b) $N_2$ adsorption-desorption isotherms; c) DFT pore size distribution.

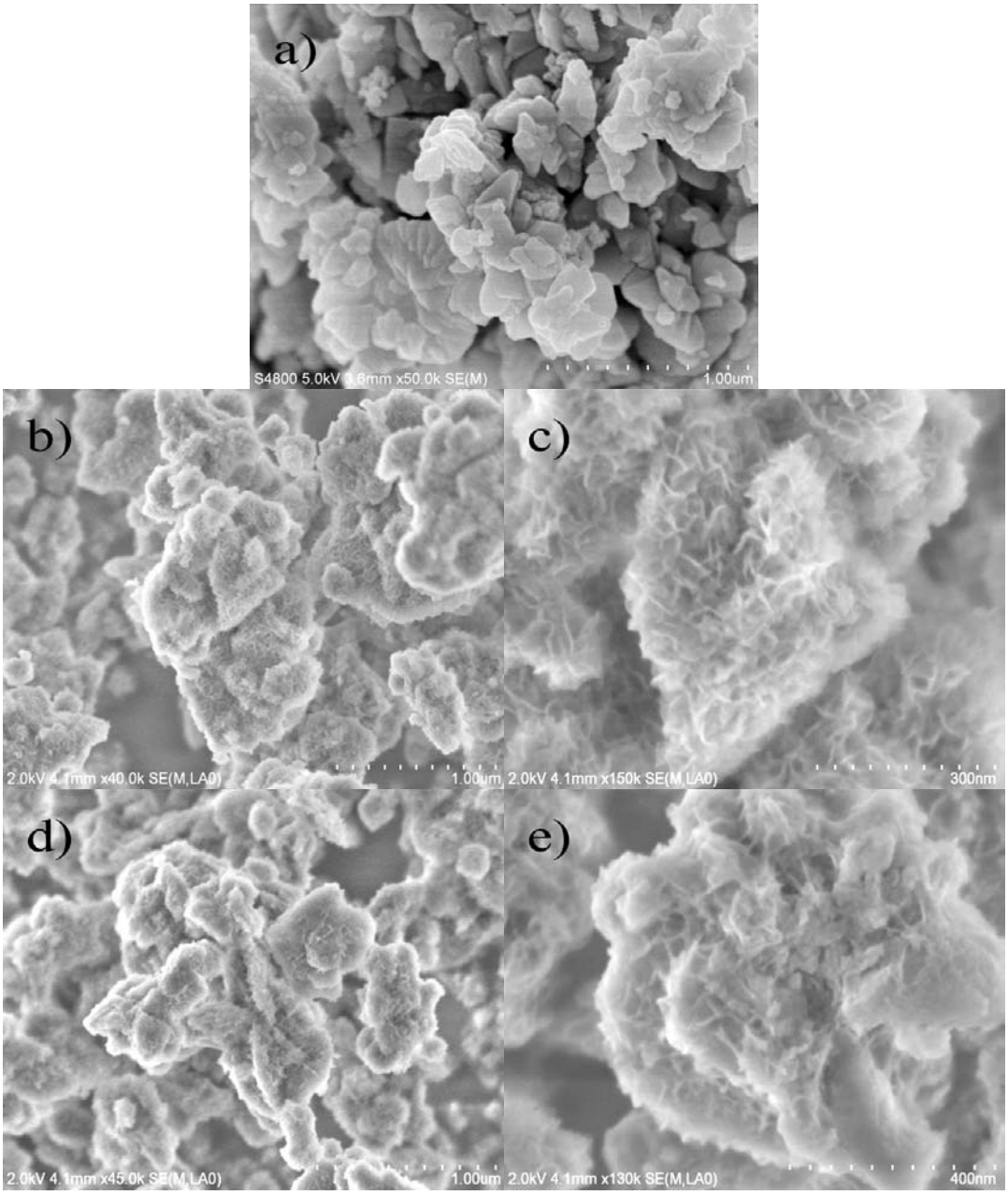


Fig. 4 – SEM image of PtSOD-M samples; a) PtSOD; b), c) PtSOD-Ni$(NO_3)_2$; d), e) PtSOD-Co$(NO_3)_2$.

The XRD results presented PtSOD-Na, PtSOD-Zn$(NO_3)_2$ and PtSOD-$ZnSO_4$ the peaks at 2Theta=13.9°and 24.3°represented (110) and (211) crystal planes, PtSOD-Zn$(NO_3)_2$, PtSOD-$ZnSO_4$ maintain well consisted of peaks that were typical of sodalite Fig. 3.a). PtSOD-Zn$(NO_3)_2$ and PtSOD-$ZnSO_4$ samples exhibited isotherms with a H3 type hysteresis loop [Fig.3.b)]. As described in Table 1 report that in the PtSOD-$Zn^{2+}$ series, the PtSOD-Zn$(NO_3)_2$ has the highest surface area of 106 $m^2/g$ and the single point pore volume is 0.44 $cm^3g^{-1}$.

SEM images [Fig. 4.a) PtSOD. b) c) PtSOD-Ni$(NO_3)_2$. d).e) PtSOD-Co$(NO_3)_2$] revealed the presence of particles of irregular petal shape and crystal size with an average diameter of 0.2-0.5μm. Also they clearly showed that no physically isolated crystals or particles of the two phases existed in the product. The PtSOD-Na after ion exchange teatment formed PtSOD-M; their shape has well preserved no distorting and collapsing. The PtSOD-M particles are numerous nanocrystals aggregated with rough surface which differ from PtSOD-Na smooth surface and PtSOD-M with higher surface area than PtSOD-Na.

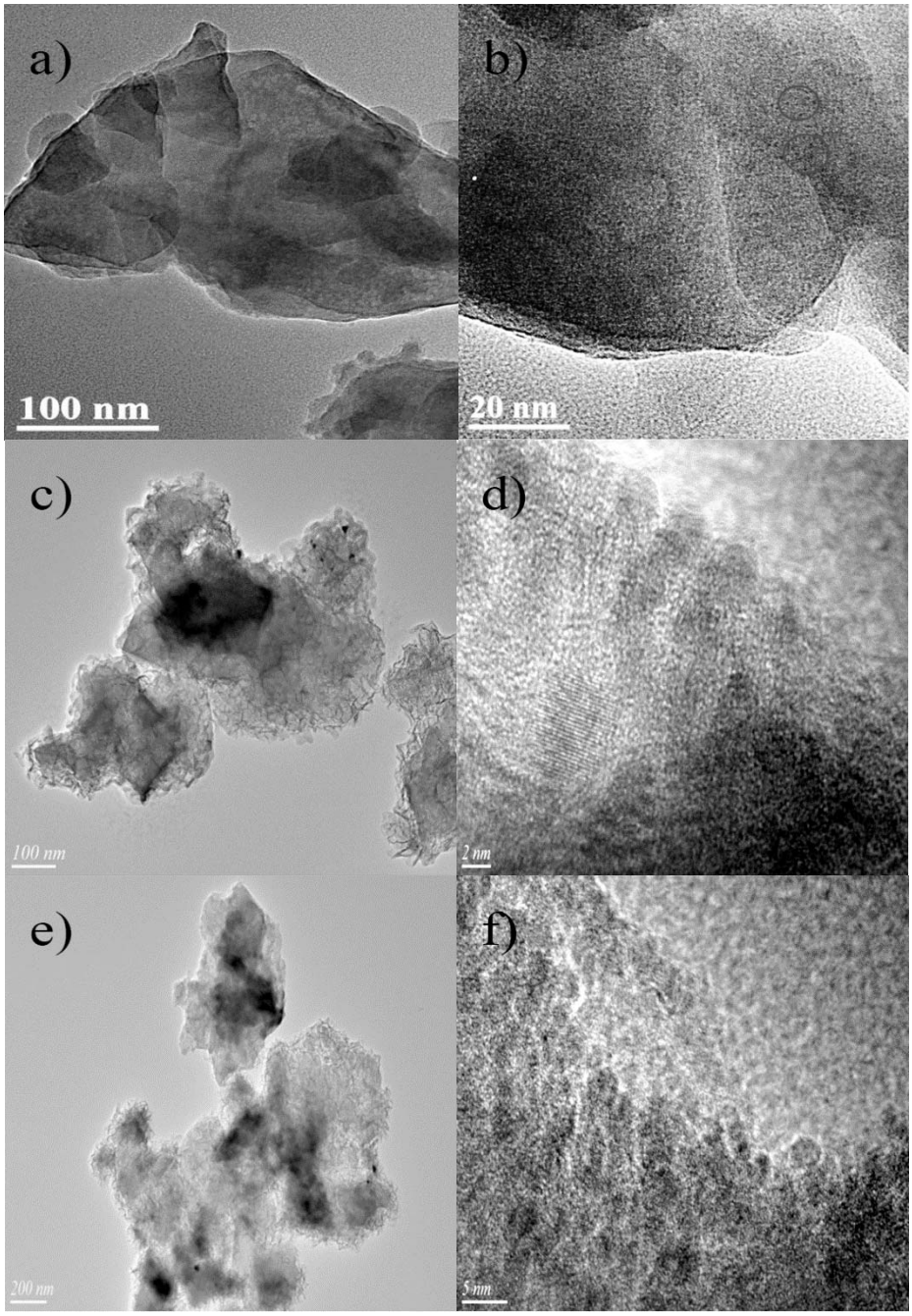


Fig. 5 – TEM image of PtSOD-M samples; a), b) PtSOD; c), d). PtSOD-Ni$(NO_3)_2$; e), f) PtSOD-Co$(NO_3)_2$.

TEM images [Fig. 5 a), b) PtSOD c), d). PtSOD-Ni$(NO_3)_2$ e), f) PtSOD-Co$(NO_3)_2$]. In Fig. 5 TEM micrograms the small clusters of platinum nanoparticles were observed and no obvious agglomeration of platinum nanoparticles. The platinum nanoparticle diameter varied between 1 and 2 nm and the mean particle size was ~1.5 nm. Fig.5.d), f) bright-field and dark-field intersect each other revealing that PtSOD-Ni$(NO_3)_2$ and PtSOD-Co$(NO_3)_2$ possessed disordered mesoporous structures. The bright-field of Fig. 5.f) showed clear that Pt nanoclusters present as small uniform in size and distributed throughout zeolite crystallites. The PtSOD-M sample was built with a much thinner framework than the PtSOD-Na sample. The thin framework of PtSOD-M also provided a higher surface area and a larger pore volume. The microporous unique lattice fringes can be observed on TEM images, that original pore structure persists or part of the reservation, on this basis and the formation of a new mesoporous structure.

*Table 1*

Surface area and pore volume analysis of of PtSOD exchange with $Ni^{2+}$, $Co^{2+}$ and $Zn^{2+}$

| Samples | Total BET surface area ($m^2/g$) | Mesopore surface area ($m^2/g$) | Micropore surface area ($m^2/g$) | Pore volume ( $cm^3/g$ ) | Pore width (nm) |
|---|---|---|---|---|---|
| PtSOD-Na | 26.4 | 26.4 | 0 | / | / |
| PtSOD-$CoCl_2$ | 68.3 | 68.3 | 0 | 0.19 | 4.9 |
| PtSOD-$Co(NO_3)_2$ | 93.6 | 93.6 | 0 | 0.30 | 6.1 |
| PtSOD-$Co(CH_3COO)_2$ | 97.9 | 97.9 | 0 | 0.24 | 6.1 |
| PtSOD-$CoSO_4$ | 71.7 | 71.7 | 0 | 0.19 | 6.1 |
| PtSOD-$NiCl_2$ | 86.0 | 86.0 | 0 | 0.24 | 4.9 |
| PtSOD-$Ni(NO_3)_2$ | 105.2 | 105.2 | 0 | 0.26 | 4.9 |
| PtSOD-$Ni(CH_3COO)_2$ | 114.6 | 114.6 | 0 | 0.24 | 4.9 |
| PtSOD-$Zn(NO_3)_2$ | 106.0 | 106.0 | 0 | 0.44 | 8.1 |
| PtSOD-$ZnSO_4$ | 73.7 | 73.7 | 0 | 0.21 | 5.1 |

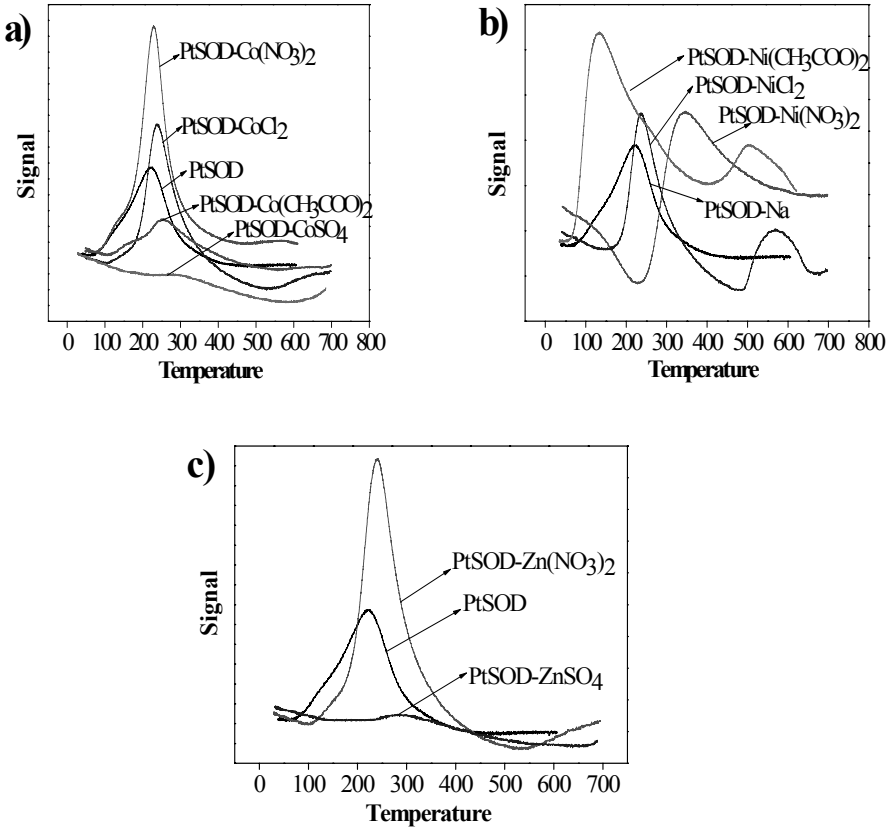


Fig. 6 – Temperature programmed desorption of hydrogen ($H_2$-TPD) of PtSOD-M.

Summarizing the data above exhibited that except for PtSOD-$NiSO_4$, PtSOD- $Zn(CH_3COO)_2$ and PtSOD-$ZnSO_4$, resulted PtSOD-M framework which is consistent with conventional sodalite counterparts. XRD patterns correspond well to the crystalline sodalite and suggested that the sodalite structure was retained after ion exchange and calcination steps. Table 1 represents the structural and textural properties of the materials. The higher specific surface area and larger pore volume were attributed to the presence of highly mesoporous structures in the PtSOD-M. The PtSOD-$Ni(CH_3COO)_2$ sample showed the highest surface area (114.6 $m^2/g$) and the PtSOD-$Zn(NO_3)_2$ showed the largest pore volume (0.44 $cm^3/g$). According to the nitrogen adsorption image and data the formation of mesoporous mainly arises from interparticle interactions.

The catalyst adsorption of $H_2$ ability was analyzed by temperature programmed desorption of hydrogen. The accessibility of the hydrogen molecules on the platinum (Pt) clusters was evaluated by $H_2$ chemisorption. This test indicating that the $H_2$ accessible into the cages of sodalite and direct contact with the encapsulated Pt active sites in the cages, also confirmed that PtSOD-M series of catalysts could be used as hydrogenation catalyst. A broad hydrogen desorption band was observed in the temperature region 50°C–700 °C, indicating the presence of weak, medium and strong hydrogen adsorption temperature sites (Fig 6.). The H-ZSM-5 showed similar hydrogen adsorption ability to Pt free sodalite material (SOD-Na). Temperature programmed was conducted to compare synthesized PtSOD-M material hydrogen adsorption ability and hydrogen spillover ability of the catalyst. The major peaks were present at 220 °C-260 °C, indicating a suitable hydrogen spillover temperature range. Desorption of hydrogen. Fig. 6.a) illustrates the $H_2$-TPD profile of PtSOD-Co series with the single peak profile in comparison to PtSOD-Na, exhibits the PtSOD-$Co(NO_3)_2$ maximum desorption (0.94mL/g) and PtSOD-$Co(CH_3COO)_2$ minimum desorption (0.43 mL/g) (Table 2). Figure.6.c) shows the $H_2$-TPD curves of PtSOD-Zn series, the maximum amount of PtSOD-Zn series PtSOD-$Zn(NO_3)_2$ hydrogen adsorption is 1.02 mL/g (Table 2). Fig. 1.b) provides information about the $H_2$-TPD curves of PtSOD-Ni series, PtSOD-$Ni(CH_3COO)_2$ and PtSOD-$NiCl_2$ the peak at ~500 °C is not commonly observed in series of PtSOD-M. The platinum nanoclusters (<1 nm) are encaged inside the sodalite cages and deep inside PtSOD-M. Due to the Ni ion exchange and the effect of high temperature more Pt sites which could contact with hydrogen molecules so the high temperature peak appeared.

*Table 2*

Benzene hydrogenation activity and hydrogen adsorption amount of PtSOD samples after exchange with $Ni^{2+}$, $Co^{2+}$ and $Zn^{2+}$

| Samples | The amount of hydrogen adsorption (mL/g) | Conversion of benzene (%)[a] |
|---|---|---|
| SOD-Na | 0 | 0 |
| H-ZSM-5 | 0 | 0 |
| PtSOD-Na | 0.33 | 0 |
| PtSOD-Na&HZSM-5 | 0.70 | 55.2 |
| PtSOD-$CoCl_2$ | 0.93 | 49.8 |
| PtSOD-$Co(NO_3)_2$ | 0.94 | 58.7 |
| PtSOD-$Co(CH_3COO)_2$ | 0.43 | 85.4 |
| PtSOD-$CoSO_4$ | 0 | 0 |
| PtSOD-NiCl2 | 0.92 | 56.9 |
| PtSOD-$Ni(NO_3)_2$ | 1.28 | 82.9 |

*Table 2 (continued)*

| | | |
|---|---|---|
| PtSOD-Ni$(CH_3COO)_2$ | 2.26 | 91.5 |
| PtSOD-Zn$(NO_3)_2$ | 1.02 | 23.0 |
| PtSOD-$ZnSO_4$ | 0 | 0 |

[a] Determined by GC using the area normalization method

Hydrogenation of benzene conversion was catalyzed by PtSOD-M catalysts. The activity of PtSOD-M was compared with PtSOD-Na with samples before ion exchange, SOD-Na and H-ZSM-5. The conversion of benzene is listed in Table 2. The results substantiate the fact that microporous PtSOD-Na without spillover hydrogen receptor providing high surface area as hydrogen spillover receptor the hydrogen spillover reaction could not happen. PtSOD-Ni$(CH_3COO)_2$ was the most active catalyst (91.5%) followed by PtSOD-Co$(CH_3COO)_2$ (85.4%), PtSOD-Ni$(NO_3)_2$ (82.9%), and PtSOD-Co$(NO_3)_2$ (58.7%) with 3 h reaction at 373K. The higher activity of PtSOD-Zn$(CH_3COO)_2$ was attributed to the mesoporous structure formed by ion exchange provides a large surface area which promoted the diffusion of benzene. PtSOD-Na has no catalytic activity caused by the too low external area of PtSOD-Na to form the hydrogen spillover. When PtSOD-Na mix with H-ZSM-5 spillover hydrogen receptors in 1:1 mass ratio, PtSOD&H-ZSM-5 showed comparatively low activity the conversion of benzene is 55.2%. Although after ion exchange the samples of PtSOD-$CoSO_4$, PtSOD-$ZnSO_4$ have mesoporous structure and with high surface area but the structure of channels can be destroyed and block hydrogen diffusion to Pt sites located inside the SOD cage. From the reaction results can also be seen the loss of catalytic activity of samples of PtSOD-$CoSO_4$, PtSOD-$ZnSO_4$. The remaining PtSOD-M except for PtSOD-$CoSO_4$, PtSOD-$ZnSO_4$ have considerable hydrogenation catalytic activity. It is not hard to deduce that PtSOD-Ni$(CH_3COO)_2$ sample has higher BET surface area and a larger pore structure, which were more conducive to the transfer material and a more favorable reaction occurs.

## CONCLUSIONS

The Pt encapsulated mesoporous sodalite catalytic material investigated in this study contains a mesoporous–microporous hierarchical structure. It showed about a 5-fold higher surface area and about a 7-fold the amount of hydrogen adsorption higher than PtSOD. Its higher BET surface area and the larger pore structure were more conducive to the transfer material and a more favorable reaction occurs. And, Pt encapsulated mesoporous sodalite catalytic material is a stable and versatile basic catalyst for a range of bulky and small molecular reactions. Given its now established physicochemical properties, it can also be used as a stable support for further surface modifications, which will expand its applicability.

*Acknowledgements*. This work was supported by the Natural Science Foundation of Shanxi Province (2014011012-4).

## REFERENCES

1. A. Corma, *Chem. Rev.*, **1997**, *97*, 2373.
2. A. Corma, *J. Catal.*, **2003**, *215,* 294.
3. J. X. Jiang, J. L. Jorda, J. H. Yu, L. A. Baumes, E. Mugnaioli, M. J. Diaz-Cabanas, U. Kolb and A. Corma, *Science.*, **2011**, *333*, 1131.
4. J. C. Kim, T. W. Kim, Y. Kim, R. Ryoo, S. Y. Jeong and C. U. Kim, *Appl. Catal. B-Environ.*, **2017**, *206*, 490.
5. L. Wang, Z. H. Diao, Y. J. Tian, Z. Q. Xiong and G. Z. Liu, *Energ. Fuel.*, **2016**, *30*, 6977.
6. F. M. Mota, P. Eliasova, J. Jung and R. Ryoo, *Catal. Sci. Technol.*, **2016**, *6*, 2735.
7. C. Kim, K. Cho, S. K. Kim, E. K. Lee, J.-N. Kim and M. Choi, *Microporous. Mesoporous. Mater.*, **2017**, *239*, 310.
8. Y.-N. Kim, M. Y. Kim and M. Choi, *Chem. Eng. J.*, **2016**, *289*, 423.
9. G. Li, J. Edwards, A. F. Carley and G. J. Hutchings, *Catal. Today.*, **2006**, *114*, 369.
10. J. K. Edwards, A. Thomas, B. E. Solsona, P. Landon, A. F. Carley and G. J. Hutchings, *Catal. Today.*, **2007**, *122*, 397.
11. E. N. Ntainjua, M. Piccinini, J. C. Pritchard, J. K. Edwards, A. F. Carley, C. J. Kiely and G. J. Hutchings, *Catal. Today.*, **2011**, *178*, 47.
12. S. J. Freakley, M. Piccinini, J. K. Edwards, E. N. Ntainjua, J. A. Moulijn and G. J. Hutchings, *Acs. Catal.*, **2013**, *3*, 487.
13. J. K. Edwards, J. Pritchard, L. Lu, M. Piccinini, G. Shaw, A. F. Carley, D. J. Morgan, C. J. Kiely and G. J. Hutchings, *Angew. Chem. Int. Ed. Engl.*, **2014**, *53*, 2381.

14. S. J. Freakley, R. J. Lewis, D. J. Morgan, J. K. Edwards and G. J. Hutchings, *Catal. Today.*, **2015**, *248*, 10.
15. J. Wang, S. A. Kondrat, Y. Wang, G. L. Brett, C. Giles, J. K. Bartley, L. Lu, Q. Liu, C. J. Kiely and G. J. Hutchings, *Acs. Catal.*, **2015**, *5*, 3575.
16. A. Akram, S. J. Freakley, C. Reece, M. Piccinini, G. Shaw, J. K. Edwards, F. Desmedt, P. Miquel, E. Seuna, D. J. Willock, J. A. Moulijn and G. J. Hutchings, *Chem. Sci.*, **2016**, *7*, 5833.
17. D. I. Enache, D. Barker, J. K. Edwards, S. H. Taylor, D. W. Knight, A. F. Carley and G. J. Hutchings, *Catal. Today.*, **2007**, *122*, 407.
18. X. Liu, M. Conte, M. Sankar, Q. He, D. M. Murphy, D. Morgan, R. L. Jenkins, D. Knight, K. Whiston, C. J. Kiely and G. J. Hutchings, *Appl. Catal. A.*, **2015**, *504*, 373.
19. R. Armstrong, G. Hutchings and S. Taylor, *Catalysts*, **2016**, 6.
20. Y. Dai, B. Lim, Y. Yang, C. M. Cobley, W. Li, E. C. Cho, B. Grayson, P. T. Fanson, C. T. Campbell, Y. Sun and Y. Xia, *Angew. Chem. Int. Ed. Engl.*, **2010**, *49*, 8165.
21. M. J. Lee, J. S. Kang, Y. S. Kang, D. Y. Chung, H. Shin, C. Y. Ahn, S. Park, M. J. Kim, S. Kim, K. S. Lee and Y. E. Sung, *Acs. Catal.*, **2016**, *6*, 2398.
22. Y. F. Zhai, O. Baturina, D. Rarnaker, E. Farquhar, J. St-Pierre and K. Swider-Lyons, *J. Phys. Chem. C.*, **2015**, *119*, 20328.
23. C. Kohler, L. Bleck, M. Frei, R. Zengerle and S. Kerzenmacher, *Chemelectrochem.*, **2015**, *2*, 1785.
24. M. I. Awad, M. M. Saleh and T. Ohsaka, *J. Solid. State. Electr.*, **2015**, *19*, 1331.
25. G. E. Michael Wiebcke, Juergen Felsche, Paul Bernd Kempa, Peter Sieger, Juerg Schefer, Peter Fischer, *J. Phys. Chem.*, **1992**, *96*, 392.
26. J. F. Guenter Engelhardt, Peter Sieger, *J. Am. Chem. Soc.*, **1992**, *114*, 1173.
27. H.-P. Zhou, H.-S. Wu, J. Shen, A.-X. Yin, L.-D. Sun and C.-H. Yan, *J. Am. Chem. Soc.*, **2010**, *132*, 4998.
28. J. Shi, L. Chen, N. Ren, Y. Zhang and Y. Tang, *Chem. Commun. (Camb).*, **2012**, *48*, 8583.
29. M. G. Sibi, A. Rai, M. Anand, S. A. Farooqui and A. K. Sinha, *Catal. Sci. Technol.*, **2016**, *6,* 1850.
30. G. V. Shanbhag, M. Choi, J. Kim and R. Ryoo, *J. Catal.*, **2009**, *264*, 88.
31. S. Shirani Lapari, Z. Ramli and S. Triwahyono, *J. Chem.*, **2015**, 1.
32. J. A. Zhu, J. A. Wu, Y. Wang and C. G. Meng, *J. Mater. Sci*, **2010**, *45*, 6769.
33. R. Kimura, J. Wakabayashi, S. P. Elangovan, M. Ogura and T. Okubo, *J. Am. Chem. Soc.*, **2008**, *130*, 12844.
34. N. Hiyoshi, *Appl. Catal. A.*, **2012**, *419-420*, 164.
35. A. Sachse, A. Galarneau, F. Di Renzo, F. O. Fajula and B. Coq, *Chem. Mater.*, **2010**, *22*, 4123.
36. J. Aguado, J. L. Sotelo, D. P. Serrano, J. A. Calles and J. M. Escola, *Energy Fuels.*, **1997**, *11*, 1225.
37. Y. M. Fang and H. Q. Hu, *J. Am. Chem. Soc.*, **2006**, *128,* 10636.
38. W. Fan, M. A. Snyder, S. Kumar, P. S. Lee, W. C. Yoo, A. V. McCormick, R. L. Penn, A. Stein and M. Tsapatsis, *Nat. Mater.*, **2008**, *7*, 984.
39. M. R. Li, I. N. Oduro, Y. P. Zhou, Y. Huang and Y. M. Fang, *Microporous, Mesoporous Mater.*, **2016**, *221*, 108.
40. M. Choi, K. Na, J. Kim, Y. Sakamoto, O. Terasaki and R. Ryoo, *Nature.*, **2009**, *461*, 246-249.
41. K. Na, C. Jo, J. Kim, K. Cho, J. Jung, Y. Seo, R. J. Messinger, B. F. Chmelka and R. Ryoo, *Science.*, **2011**, *333*, 328.
42. J. Garcia-Martinez, M. Johnson, J. Valla, K. H. Li and J. Y. Ying, *Catal. Sci. Technol.*, **2012**, *2*, 987.
43. H. G. Peng, L. Xu, H. H. Wu, Z. D. Wang, Y. M. Liu, X. H. Li, M. Y. He and P. Wu, *Microporous, Mesoporous. Mater.*, **2012**, *153*, 8.
44. J. Zhu, Y. Zhu, L. Zhu, M. Rigutto, A. van der Made, C. Yang, S. Pan, L. Wang, L. Zhu, Y. Jin, Q. Sun, Q. Wu, X. Meng, D. Zhang, Y. Han, J. Li, Y. Chu, A. Zheng, S. Qiu, X. Zheng and F. S. Xiao, *J. Am. Chem. Soc.*, **2014**, *136*, 2503.
45. T. Xue, H. P. Liu, Y. Zhang, H. H. Wu, P. Wu and M. Y. He, *Microporous, Mesoporous. Materials.*, **2017**, *242*, 190.
46. R. A. Naikoo, S. U. Bhat, M. A. Mir and R. Tomar, *Microporous, Mesoporous. Mater.*, **2017**, *243*, 229.
47. A. M. Fonseca and I. C. Neves, *Microporous, Mesoporous Mater.*, **2013**, *181*, 83.
48. S.Eiden-Assmann, *Mater. Res. Bull.*, **2002**, *37*, 875.